A Higher Performance Electric-Arc-Driven Shock Tube

W. A. Menard

Environmental Sciences Division

The results of an experimental study made to improve the performance of electric-arc-driven shock tubes are presented. With only minor modifications to the driver, shock velocities have been increased by a factor of 3. The new driver has a conical internal design of small volume, and uses a light-weight diaphragm which disintegrates during the electrical discharge. Data obtained from a 15.2-cm-diameter driven tube, 11.3 m in length, show little shock wave attenuation in gases simulating the Jupiter and Saturn atmospheres. Shock velocities of 45 km/s with test times in excess of 4 μs have been attained. Because of the extended performance, the electric-arc-driven shock tube may now be used to study many outer-planet atmospheric entry problems.

Introduction

To study Jupiter and Saturn atmospheric entry problems in the laboratory requires a facility capable of producing shock velocities from 25 to 48 km/s. The purpose of this article is to report on the modifications made to the JPL shock tube, which have increased velocity well into the outer-planet entry range. An experiment was designed to investigate performance over a wide range of driver energies, and initial pressures from 6.66 to 6660 N/m^2 (0.05 to 50 torr).[1] Measurements of shock velocity, shock wave attenuation, and test time were made in several test gases.

Facility

The JPL electric-arc-driven shock tube was originally designed with a 3.5-cm-diameter driver, 66 cm long (Reference 1). A later design (Reference 2) provided for a variable length and increased the diameter to

[1]Where applicable, the International System of Units is stated first, followed by the customary units in parentheses. In each case, the value in parentheses represents the measured or calculated unit.

15.2 cm. Energy for the driver is supplied by a 100-capacitor (14.5 μF) storage system, rated at 290,000 J when charged to 20,000 V.

The new driver, which was designed from the driver of Reference 2 with only minor modifications, is shown in Figure 1. The cathode is a 3.2-cm-diameter cylinder made from Mallory 1000 (a sintered tungsten alloy). A hole in the cathode tip allows the trigger wire to be pulled through. The anode is a 2.5-cm-wide, 7.6-cm-diameter copper ring located 9.6 cm from the cathode. A conical Teflon insert reduces the driver volume to 350 cm^3, and provides a fairly smooth internal contour from the cathode tip to the 15.2-cm-diameter driven tube. The half angle of the cone is approximately 217 mrad (12.5 deg). The diaphragm is located on the downstream side of the anode ring. A 0.025-cm-diameter stainless steel wire is strung across the opening, and the trigger pull wire is attached to this wire. In operation, the arc is initiated by pulling the trigger wire toward the cathode.

In order to reduce diaphragm opening losses and to insure a fast opening time, Mylar diaphragms (0.035 cm thick) are used. Helium or hydrogen gas is supplied to the driver at a pressure of 1.19×10^6 N/m^2 (11.8 atm), just 4% less than the static rupture pressure of the diaphragms.

When the arc is struck, the trigger wires and the diaphragm immediately disintegrate. It was found that at high driver energies the copper anode could not hold the arc. Severe erosion on the surface of the stainless steel transition section was evidence that the arc had extended 7 cm beyond the diaphragm. Current measurements of the capacitor bank discharge show the arc burns for about 25 μs. During this time the driver

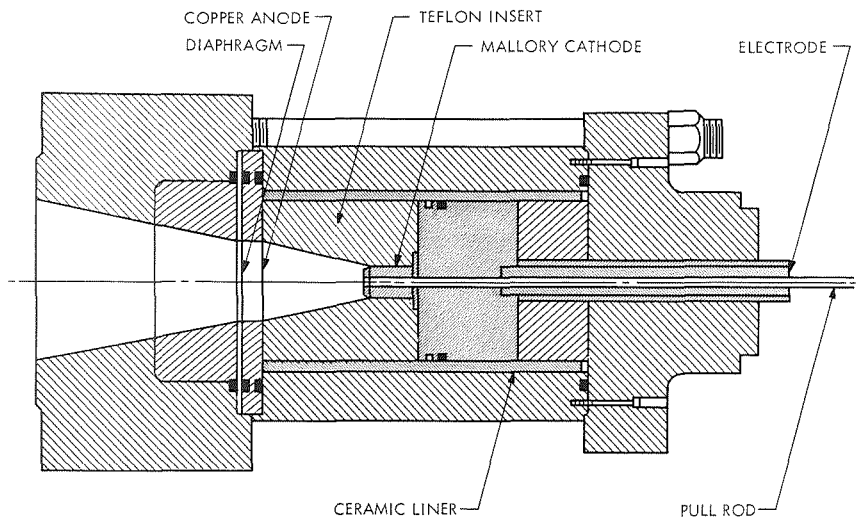

Figure 1. Schematic of driver configuration

gas can receive energy from the arc while in the driver, and as it expands down the tube.

Erosion of the cathode and copper anode was minimal. Replacing the transition section with one made of copper would reduce erosion there and improve electrode efficiency.

Shock Velocity Measurements

The most abundant elements in the atmospheres of Jupiter and Saturn are believed to be hydrogen and helium. For this reason the majority of the shock tube runs were made in a mixture of 80% He and 20% H_2 (by volume).

The driven tube was 11.3 m long and had instrument ports arranged to measure shock velocity U_s at distances L from the diaphragm of 2, 3.66, and 10.67 m. Shock speeds were measured by viewing the shock front radiation with collimated photomultipliers spaced 61 cm apart.

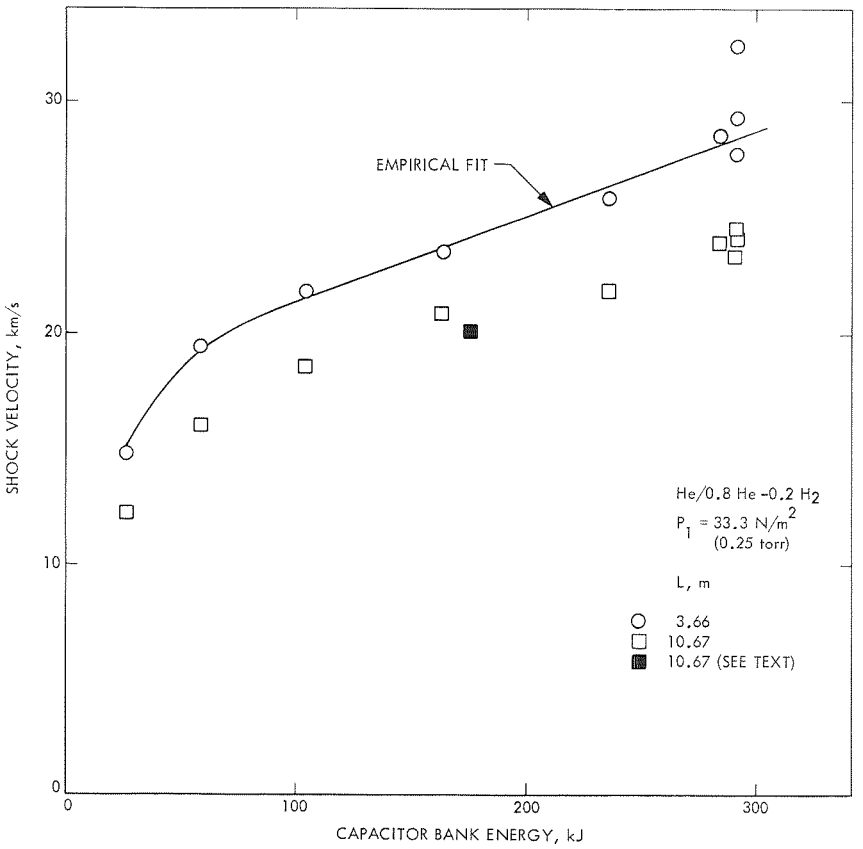

Figure 2. Variation in shock velocity with energy input

Velocities were measured to an approximate accuracy of ±3%. The tube was cleaned and pumped to 0.06 N/m² (0.5 μ) or less before each run.

Shock velocities obtained in 33.3 N/m² (0.25 torr) of the test gas, over a range of driver energies from 26,000 to 290,000 J, are presented in Figure 2. The driver gas was helium, and the data were taken at 3.66 and 10.67 m from the diaphragm. Velocities were obtained from 12 to over 32 km/s. They are seen to increase continuously as energy is increased with no indication of leveling off. If more energy were available, it would appear that even higher speeds could be reached.

The dark data point at $L = 10.67$ m was taken with one-fourth of the capacitor bank disconnected to investigate the effect of driver voltage on performance. No significant effect was observed.

The effect of initial pressure on performance is shown in Figure 3. Pressure was varied from 6.66 to 6660 N/m² (0.05 to 50 torr) while hold-

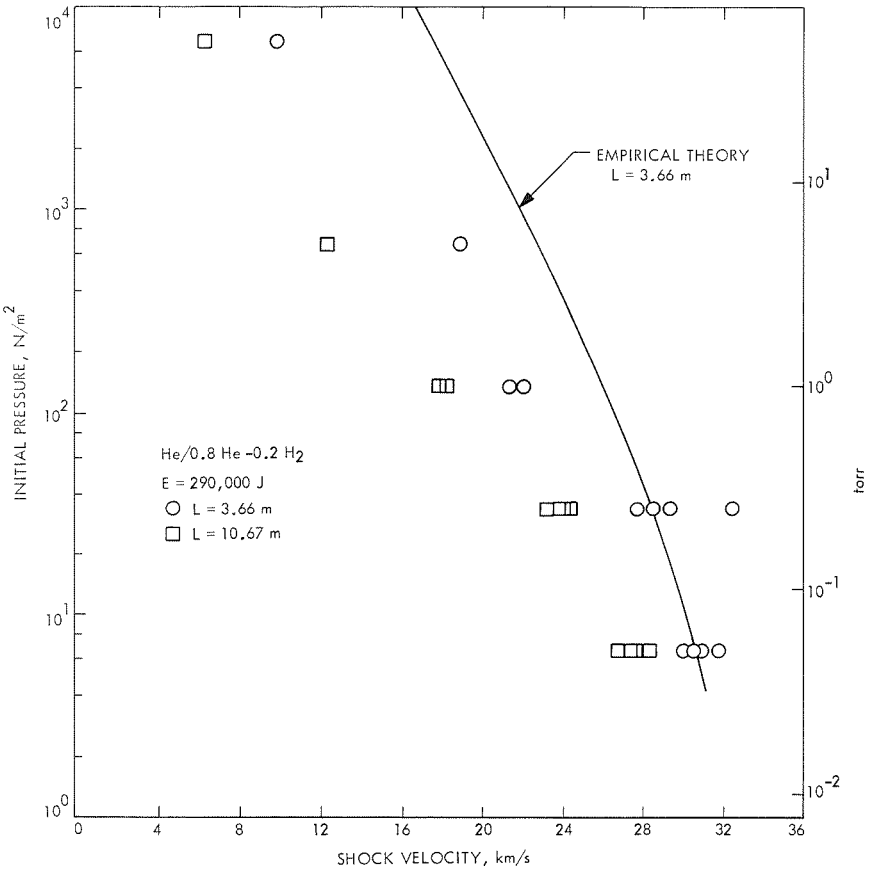

Figure 3. Shock velocity/initial pressure performance

ing energy constant. Attenuation of the shock wave is less at the lower pressures. Over a distance of 7 m, the lowest pressure data shows an attenuation of only 10%, but at pressures of 666 and 6660 N/m^2 (5 and 50 torr), the attenuation is 35%.

Other Gases

Runs were also made in pure hydrogen, helium, air, and argon, using helium and hydrogen driver gases. A summary of results is presented in Table 1. Shock velocity and test time data at two tube locations are given. The test times, in μs, are in parentheses. Where times are not shown, it is because the shock front had not completely formed.

Shock velocities, in general, decrease as molecular weight of the test gas increases. With a helium driver, shock speeds in the light gases are greater than 30 km/s, and in the heavy gases, $U_s \geq 20$ km/s. A further increase in shock velocity is obtained when hydrogen is used as the driver gas. Hydrogen-driven shock waves as fast as 45 km/s have been produced. Higher speeds were also obtained in the heavy gases, but they are accompanied by stronger attenuation.

Hydrogen is obviously more efficient in accepting electrical energy and converting it into flow energy, and damage to the driver verified its

Table 1. Shock velocity, test time, and equilibrium temperature for several driver and driven gases, measured at two distances from the diaphragm[a]

Driven gas	Helium driver gas		Hydrogen driver gas		Temperature,[b] K
	3.66 m	10.67 m	3.66 m	10.67 m	
Hydrogen	—	—	45.0* (4-7)	39.5 (6)	12,300
0.2 H_2-0.8 He	30.8 (5)	28.4 (7)	41.3* (4)	40.4 (6)	22,000
Helium	34.4* (4)	28.9 (6)	—	—	21,000
Air	27.9* (7)	23.1 (11)	32.7 —	20.3 (11)	31,000
Argon	25.7 —	20.0* (12)	31.7 —	15.8 (12)	34,700

[a]Shock velocity in km/s, test time (in parentheses) in μs; initial driven gas pressure = 6.66 N/m^2 (0.05 torr); capacitor bank energy = 2.9 x 10^5 J.

[b]For velocities with asterisk.

efficiency in absorbing energy. After several runs the Teflon insert had developed deep holes near the cathode and required replacing. The holes were apparently burned by a much hotter plasma than was generated in helium.

The final column in Table 1 shows the equilibrium temperatures calculated (Reference 3) for the asterisked data. These temperatures are extremely high for incident shock waves. In fact, comparable temperatures have not been produced in the reflected waves of other conventional shock tubes.

Test Time Measurements

Test time is the time interval between passage of the shock front and the contact surface at a point on the shock tube. Three types of measurements were made to determine test times: (1) wide-band-pass radiation measurements from the sidewall, (2) narrow-band-pass measurements from the sidewall, and (3) heat transfer measurements on a model located on the tube center line. Wide-band radiation was observed with a collimated photomultiplier having an S-11 (visible) response. The narrow-band measurements were made with a photomultiplier viewing the gas through a 5-nm (50-Å) half-width, narrow-band-pass filter. The center wavelength was selected to coincide with the intense H_α line (656.3 nm). As the test slug passed the viewing station, radiation from hydrogen would disappear upon arrival of the helium driver gas. Two calorimeter heat transfer measurements were made to verify the results from the radiation techniques. Both measurements showed a linear slope of the output which is typical of constant stagnation point heating. The temperature change at the contact surface was recorded as an abrupt voltage change in the gauge output.

Radiation Profiles

Oscillograms of strong shock waves in 6.66-N/m^2 (0.05 torr) test gases are shown in Figures 4 and 5. The top traces are narrow-band intensity profiles, I_{NB}, and the bottom traces are wide-band profiles, I_{WB}. Absolute intensity calibrations were not made but in each record the voltage outputs from I_{NB} were much less than the outputs from I_{WB}.

The oscillogram in Figure 4a is from a 30.5-km/s shock in the 0.8He–0.2H_2 mixture. Identified on the narrow-band trace are the shock front, the atomic nonequilibrium overshoot, the equilibrium level, and finally the termination of the test time by arrival of the contact surface. The equilibrium level is highly ionized, consequently there should be little H_α radiation. The radiation observed may be from the He^+ 656.0-nm

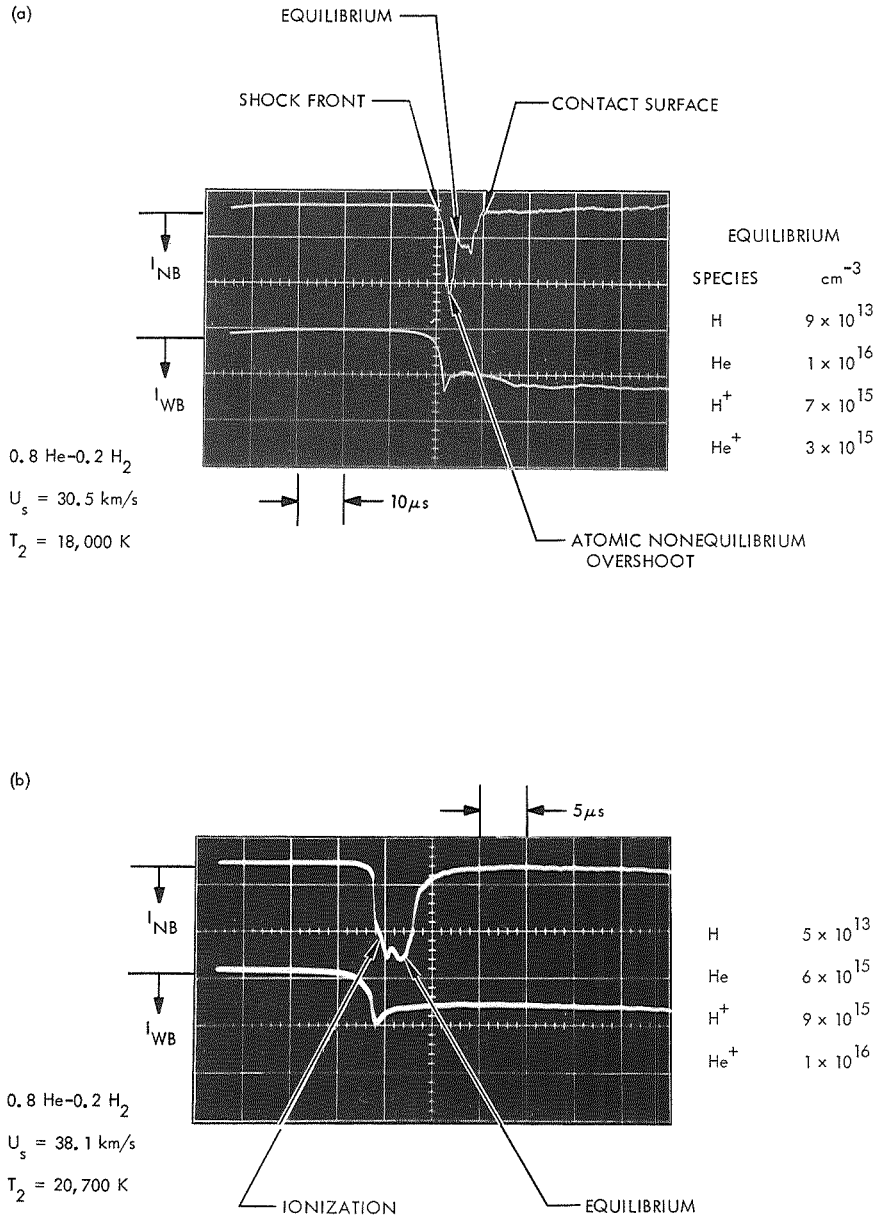

Figure 4. Narrow- and wide-band oscilloscope traces for 0.8 He–0.2 H_2 mixture

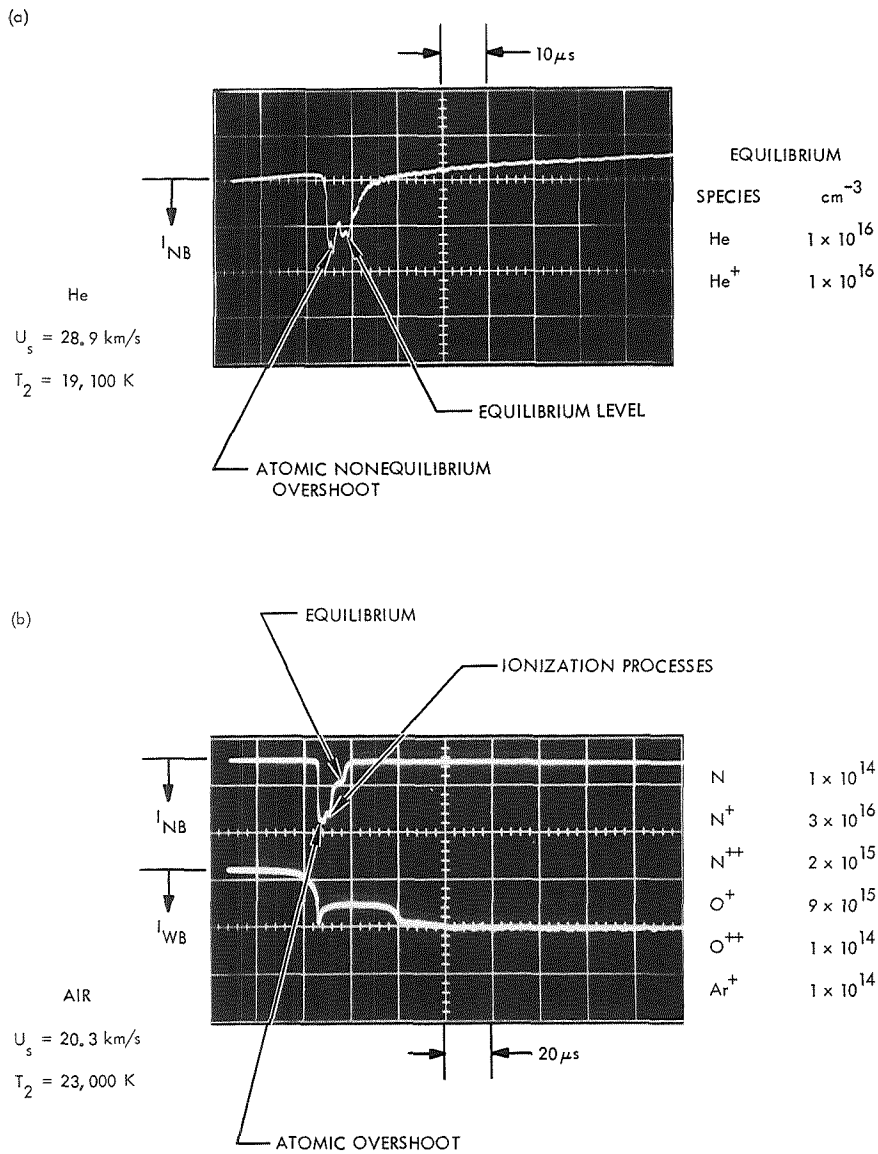

Figure 5. Narrow- and wide-band oscilloscope traces for He and air

(6560 Å) line, and the continuum. Increasing shock velocity to 38.1 km/s produces the profiles shown in Figure 4b. At this temperature the equilibrium composition is even more highly ionized. The sustained high level of equilibrium radiation may again be due to the continuum and He^+ line. Note that the helium ion number density has increased by a factor of 3 over the 30.5-km/s data. The narrow-band intensity drops sharply at the interface with the driver gas.

In Figure 5 are shown data for helium and air. Helium looks similar to the $0.8He–0.2H_2$ data. From the air trace it appears that several ionization processes are seen in the approach to equilibrium. In other runs these processes were observed to smooth out and the equilibrium level increased as temperature increased. At a temperature of 28,500 K the overshoot had disappeared and the intensity remained constant from the shock front to the interface.

The arrival of the contact surface is not obvious on most of the wide-band intensity data but is shown clearly when observed through the H_α filter. Tests made with H_2 driver gas did not alter the appearance of the test slug radiation profiles.

Correlation of Test Time Measurements

Some of the test time measurements are given in Table 1. Test times greater than 4 μs were obtained for all test conditions of the experiment, and if our interpretation of the radiation profiles is accurate, equilibrium was established in most cases.

An attempt to correlate the data with the boundary layer theories of Mirel (References 4 and 5) was unsuccessful. Laminar theory predicts "infinitesimal" test slug lengths at our Mach numbers and pressures. If one arbitrarily applies turbulent theory, lengths equal to about 25% of those measured are calculated. Similar results have been obtained by F. Livingston of this Laboratory in a pressure-driven shock tube operated at very low initial pressures. He was able to correlate his unpublished data, however, by considering two-dimensional effects.

The present measurements were correlated to the time it takes a disturbance originating at the wall to reach the center of the tube. Plotted in Figure 6 are the calculated times, $\tau_c = r/a_2$, versus the measured test times, τ_m, for all data having $U_s \geq 18$ km/s. (The radius of the tube is r and a_2 is the speed of sound.) Data for the five test gases and three initial pressures are shown. Even though there is large scatter, the general agreement is good. It would appear that more theoretical work is needed to better understand two-dimensional effects in shock tube flows.

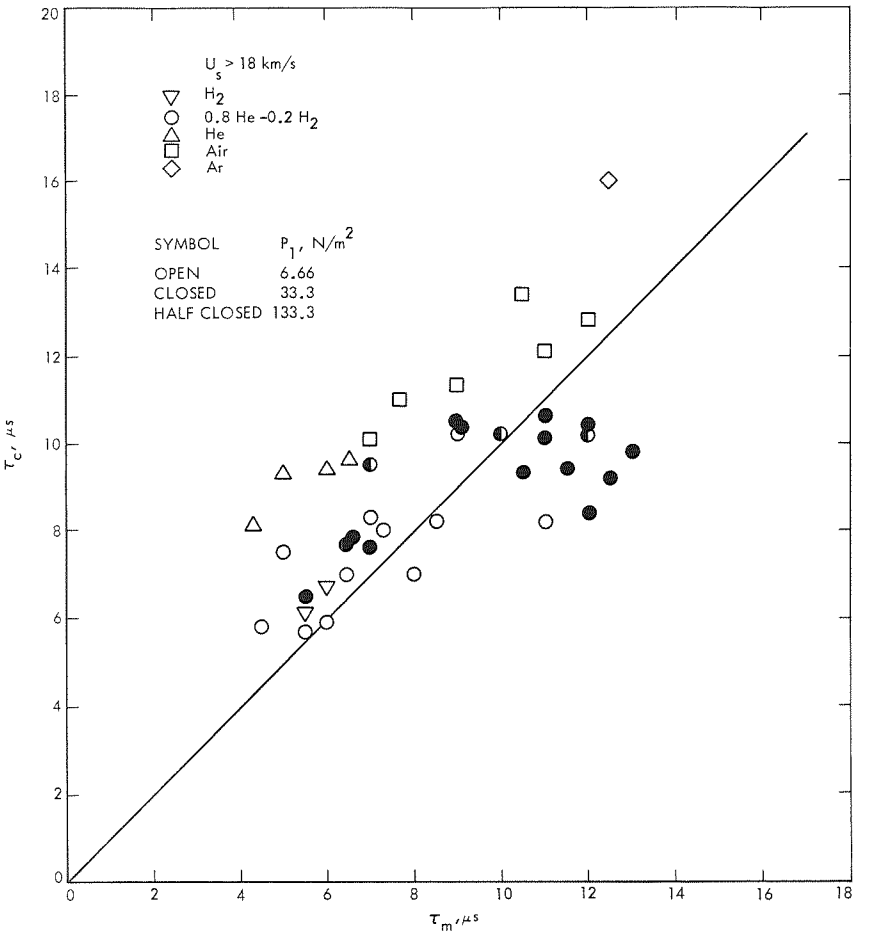

Figure 6. Correlation of test time measurements

Comparison With Other Facilities

A comparison with performance from other shock tubes is made in Figure 7. The present results are plotted for driven tube lengths from 2 to 10.67 m. The shock velocities exceed all other driving techniques except the electromagnetic driver. The modest attenuation is comparable to the combustion, piston, electrical, and two of the implosion drivers.

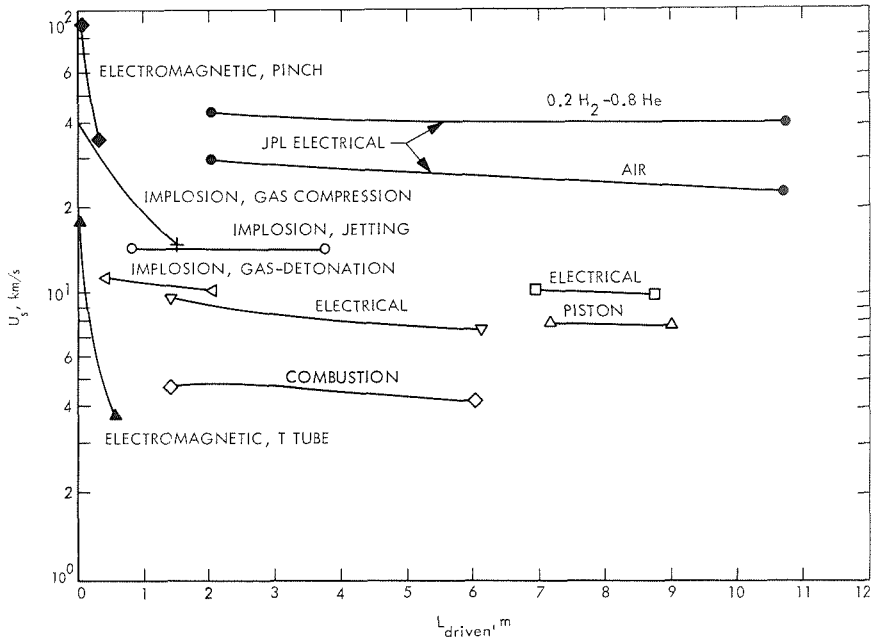

Figure 7. Comparison of present JPL performance with other driving techniques

References

1. Collins, D. J., Livingston, F. R., Babineaux, T. L., and Morgan, N. R., *Hypervelocity Shock Tube*, Technical Report 32-620. Jet Propulsion Laboratory, Pasadena, Calif., June 15, 1964.

2. Williard, J. W., "Performance of a Ceramic-Lined 6-In.-Diameter Arc Driver," Paper 68-366, AIAA 3rd Aerodynamic Testing Conference, 1968.

3. Menard, W. A., and Horton, T. E., *Shock-Tube Thermochemistry Tables for High-Temperature Gases: Vol. I. Air*, and *Vol. III. Helium, Neon, and Argon*, Technical Report 32-1408. Jet Propulsion Laboratory, Pasadena, Calif., Nov. 1, 1969 (Vol. I) and Jan. 1, 1970 (Vol. III).

References (contd)

4. Mirels, H., "Test Time in Low Pressure Shock Tubes," *Phys. Fluids*, Vol. 6, No. 9, p. 1201, 1963.

5. Mirels, H., "Shock Tube Test Time Limitation Due to Turbulent Wall Boundary Layer," *AIAA J.*, Vol. 2, No. 1, p. 84, 1964.